RSC Advances

ROYAL SOCIETY OF CHEMISTRY

www.rsc.org/advances

Room-temperature phosphorescence probe based on Mn-doped ZnS quantum dots for the sensitive and selective detection of selenite

Jialing Chen[1], Yaxian Zhu[1], Yong Zhang[2]*

[1] Department of Chemistry, College of Chemistry and Chemical Engineering, Key Laboratory of Spectrochemical Analysis & Instrumentation, Ministry of Education, Xiamen University, Xiamen 361005, China

[2] State Key Laboratory of Marine Environmental Science of China (Xiamen University), College of Environment and Ecology, Xiamen University, Xiamen 361102, China

* Corresponding Author：

Address: State Key Laboratory of Marine Environmental Science of China *(Xiamen University)*, College of Environment and Ecology, Xiamen University, 361102 Xiangan, Xiamen, Fujian Province, China.

Tel.: +86 592-2188685;

Fax: +86 592-2888685.

E-mail address: yzhang@xmu.edu.cn

Abstract

The room-temperature phosphorescence (RTP) of Mn-doped ZnS quantum dots (Mn-ZnS QDs) was quenched by the addition of selenite in the presence of glutathione. The quenching of the RTP emission of Mn-ZnS QDs was due to HSe^- ions which was the reaction product of selenite and glutathione. Based on the above finding, a simple, rapid, sensitive probe for selective detection of selenite was successfully fabricated. Under the optimal experimental conditions, a linear relationship was obtained covering the linear range of 0.1-5.0 $\mu mol \cdot L^{-1}$ and the detection limit (3σ) was 0.085 $\mu mol \cdot L^{-1}$. The proposed method was successfully applied for the determination of selenite in sodium selenite tablets and sodium selenite and vitamin E injection with satisfactory results.

Keywords: selenite; glutathione; Mn-doped ZnS quantum dots (Mn-ZnS QDs); room-temperature phosphorescence

1 Introduction

Selenium (Se) is a micronutrient that is of potential use in the prevention and treatment of disease. Twenty-five Se-proteins have been identified so far in humans [1, 2]. Most Se-proteins participate in antioxidant defence and redox state regulation, particularly the families of glutathione peroxidases and thioredoxin reductases [3]. Several human diseases including cancer, diabetes, cardiovascular and immune system disorders are associated with insufficient Se levels, and particularly Se-proteins [4]. During the last decade, humans have considered the direct intake of Se supplements. Two types of multimicronutrients can be distinguished: (i) multi-vitamins and multi-mineral preparations containing inorganic Se, other trace elements and vitamins, and (ii) supplements based on Saccharomyces cerevisiae yeast (Baker's yeast) [5, 6]. The World Health Organization recommend that the average daily intake of selenium for adults is 16 μg per day for women and 21 μg per day for men, taking into account body weight. However, care should be taken when using supplements because excessive Se intake leads to toxic effects. Some studies have been carried out showing long-term administration of as little as 200 μg per day selenium is associated with the increased incidence of type 2 diabetes [7, 8].

Selenite (SeO_3^{2-}) is the commonest chemical form of inorganic selenium, and can react with glutathione (GSH). One of the reaction products is selenidiglutathione (GSSeSG), which is a key intermediate in the selenium metabolic pathway [9, 10]. So selenite has been considered as an important Se supplementation [11]. Several methods have been reported for the quantitative determination of selenite, including

liquid chromatography inductively coupled plasma mass spectrometry [12], graphite furnace atomic absorption [13], and inductively coupled plasma atomic fluorescence spectrometry [14]. But these approaches require expensive and sophisticated instrumentation as well as complicated sample preparation processes. Therefore, there is increasing demand to develop cost-effective, easy to use, reliable and robust methods for the measurement of selenite.

Room-temperature phosphorescence (RTP) probes based on Mn-doped ZnS quantum dots (Mn-ZnS QDs) have attracted considerable attention in recent years [15-32]. The long lifetime of phosphorescence allows a suitable delay time to avoid the interferences from autofluorescence and scattering light [33]. So Mn-ZnS QDs have being used as phosphorescence probes for a great number of analytes including ions [16, 18, 34], small molecules [27, 35-40] and biomacromolecules [15, 41-44]. Xie et al. [18] fabricated a label-free aptamer with cetyltrimethylammonium bromide-capped Mn-ZnS QDs for the detection of Hg^{2+}. Wang et al. [35] combined the RTP emission of Mn-ZnS QDs and the merits of the surface imprinting polymers to develop a new type probe. The molecularly imprinted polymer based RTP probe showed good selective detection of pentachlorophenol in water. Wu et al. [41] developed a dual-channel sensing system with bovine serum albumin capped Mn-ZnS QDs: phosphorescent quenching sensing of trypsin and resonant light scattering sensing of lysozyme. Thus, Mn-ZnS QDs have become one of the most potentially useful QDs for chemical and biological sensing.

Herein, we report a new Mn-ZnS QDs probe for the RTP detection of selenite.

Selenite can react with GSH to form the highly reactive intermediate, hydrogen selenide ions (HSe^-), especially in the presence of excess GSH [45]. Besides, the HSe^- can efficiently quench the RTP of Mn-ZnS QDs. Thus, a simple and sensitive probe for detection of selenite based on the Mn-ZnS QDs has been fabricated. The proposed method was successfully applied to detect selenite in sodium selenite tablet and sodium selenite and vitamin E injection with satisfactory results.

2. Experimental

2.1. Chemicals and reagents

L-glutathione, $Zn(CH_3COO)_2 \cdot 7H_2O$, $Mn(CH_3COO)_2 \cdot 4H_2O$, and $Na_2S \cdot 9H_2O$ were purchased from Sinopharm Chemical Reagent Co., Ltd. Na_2SeO_3 was purchased from Xilong Chemical Co., Ltd. Mercaptopropionic acid (MPA) was obtained from Acros Organics. All chemicals were of analytical grade and were used as received without further purification. Sodium selenite tablets 1 were purchased from Shanghai Tiancifu Biological Engineering Co., Ltd (Shanghai, China) and Sodium selenite tablets 2 were purchased from Shandong Xili Pharmaceutical Group Co., Ltd (Shandong, China). Sodium selenite and vitamin E injection was purchased from Sichuan Weierkang Animal Pharmacy Co., Ltd (Sichuan, China). Purified water from an Elix 70 Clinical water purification system (Millipore, France) with a resistivity higher than 18.2 $M\Omega \cdot cm^{-1}$ was used to prepare all of the solutions.

2.2. Apparatus

The morphology and structure of the Mn-ZnS QDs were characterized by using a

FEI Tecnai F30 high resolution transmission electron microscope (HRTEM) with an acceleration voltage of 300 kV. RTP spectra and RTP decay curves were measured on a Cary Eclipse fluorescence spectrophotometer in the phosphorescence mode equipped with a quartz cell (1 × 1 cm) (Varian American Pty Ltd., USA). The excitation wavelength was 300 nm when the slit widths of excitation and emission were 10 nm and 20 nm, respectively. The PMT voltage was set at 600 V. For the lifetime measurements, the initial delay time was set at 0.2 ms while the gate time was typically set at 5.0 ms. The Fourier Transform infrared (FTIR) spectra (4000-400 cm^{-1}) in KBr were recorded on a Nicolet 380 FTIR spectrometer (Thermo Fisher Scientific, USA). The X-ray diffraction (XRD) spectra were collected on a Rigaku Ultima IV X-ray diffractometer (Rigaku, Japan).

2.3. Synthesis of the Mn-ZnS QDs

The Mn-ZnS QDs were prepared on the basis of a published procedure with minor modifications [33, 46]. In a 250 mL three-necked flask, 100 mL of 0.04 $mol \cdot L^{-1}$ MPA, 10 mL of 0.1 $mol \cdot L^{-1}$ $Zn(CH_3COO)_2$, and 4 mL of 0.01 $mol \cdot L^{-1}$ $Mn(CH_3COO)_2$ were sequentially added. The mixed solution was adjusted to a pH of 11 with 1 $mol \cdot L^{-1}$ NaOH. After stirring at room temperature for 30 min in nitrogen, 10 mL of 0.1 $mol \cdot L^{-1}$ Na_2S was quickly injected into the solution. The mixture was stirred for another 20 min, and then the solution was aged at 50 °C under open-air conditions for 2 h to form MPA-capped Mn-ZnS QDs. The quantum dots were precipitated with acetone, centrifuged, washed with acetone, and finally dried in a vacuum.

2.4. Measurement procedures

For the determination of selenite, 100 μL of 1.2 $g \cdot L^{-1}$ Mn-ZnS QDs, 1 mL of 0.1 $mol \cdot L^{-1}$ Tris-HCl buffer solution (pH 7.4), 250 μL of 10 $mmol \cdot L^{-1}$ GSH, and 1 mL of 10 $\mu mol \cdot L^{-1}$ selenite or 1 mL of real samples were added to a 10 mL calibrated test tube. The mixture was diluted to the mark with purified water, mixed thoroughly. The mixture was taken to phosphorescence measurement at the excitation wavelength of 300 nm. The phosphorescence intensity at the maximum phosphorescence wavelength was used for quantification.

2.5. Sample treatment

Five sodium selenite tablets were weighed and powdered. 0.15 g of the powder was dissolved in water and subjected to ultrasonification for 30 min. Then, the solution was filtrated to remove the insoluble precipitates. The filtrated stock solution was transferred into a 100 mL volumetric flask, and then the sample was diluted to the mark with purified water. 0.2 mL of sodium selenite and vitamin E injection was transferred into a 100 mL volumetric flask and then diluted to the mark with Milli-Q water. The standard sample was subjected to ultrasonification for 30 min. The stock solution was used for further quantitative detection.

3. Results and discussion

3.1. Characterization of the Mn-ZnS QDs

The HRTEM image of the Mn-ZnS QDs is shown in Fig. 1. The image reveals that the Mn-ZnS QDs are spherical and dispersed with an average diameter of 3.5 nm. Meanwhile, the XRD spectra were scanned at 2θ from 5° to 80°. The XRD pattern of

the Mn-ZnS QDs is shown in Fig. S1, and it exhibits a zinc-blend structure with peaks for (111), (220), and (311) planes. Fig. S2 depicts the FTIR spectra of the MPA-capped Mn-ZnS QDs and the free ligands MPA. The strong peaks at 1562 and 1398 cm^{-1} correspond to the signifying of C=O and C-OH stretching [39]. The disappearance of the S-H (2571 cm^{-1}) stretching vibrational peak in the FTIR spectra of MPA capped Mn-ZnS QDs indicates that the MPA had combined onto the surface of the nanocrystals through thiols. The RTP spectrum of QDs show a maximum excitation peak at 300 nm and a narrow emission band around 590 nm, which is relatively independent of the size of the nanoparticles, could be attributed to the triplet transition ($^4T_1$-$^6A_1$) emission of the Mn^{2+} impurity [47].

Insert Fig. 1 here

3.2. Factors affecting the sensitivity of the RTP detection of selenite

The factors that may influence the reactions were studied to achieve the sensitive detection of selenite. The effect of GSH on the RTP quenching efficiency of Mn-ZnS QDs was tested with 5 μmol·L^{-1} selenite in Tris-HCl (pH 7.4, 10 mmol·L^{-1}). As shown in Fig.2, in the beginning, the quenching efficiency increased rapidly when the concentration of GSH was increased. Then it reached the maximum at the concentration of 0.25 mmol·L^{-1}. It decreased a little when the concentration exceeded 0.25 mmol·L^{-1}. Therefore, 0.25 mmol·L^{-1} GSH was selected as optimum and used in the subsequent detection process.

Insert Fig. 2 here

The RTP quenching efficiency of the Mn-ZnS QDs in the presence of 0.25

mmol·L^{-1} GSH and 5 μmol·L^{-1} selenite was pH-dependent. As shown in Fig. 3, the RTP quenching efficiency leveled off at pH values from 5.0 to 7.4, and then gradually decreased at pH values from 8.0 to 9.0. The reaction of selenite with GSH was active in neutral and acidic solution [48]. So, the RTP quenching efficiency was high when pH values lower than 7.4. But the Mn-ZnS QDs were unstable in acidic solution [16]. Therefore, a pH of 7.4 was used in the experiment.

Insert Fig. 3 here

3.3. Analytical performances

To explore the potential application of the Mn-ZnS QDs for RTP detection, the effect of selenite on the RTP of the Mn-ZnS QDs in the presence of GSH was investigated. Under the optimal experimental conditions, the RTP intensity of the Mn-ZnS QDs gradually decreased as the concentration of selenite increased. The RTP quenching response of the Mn-ZnS QDs to selenite in an aqueous solution is shown in Fig. S3.

As shown in Fig. 4, a linear calibration plots of the quenched RTP intensity against the concentration of selenite was observed in the range of 0.1-5.0 μmol·L^{-1} (R^2=0.9940). The detection limit (3σ) for selenite was 0.085 μmol·L^{-1}, and the relative standard deviation was 1.2% for 11 replicate detections of 1.0 μmol·L^{-1} selenite. The analytical performance for the detection of selenite using the proposed method has been compared with that of previous reports, and the results are listed in Table 1 [49-51]. It can be seen that the proposed method showed lower detection limit than other analytical techniques.

Insert Fig. 4 here

Insert Table 1 here

3.4. Selectivity of the Mn-ZnS QDs-based RTP method

The selectivity of the developed RTP probe was assessed by studying the effect of different potential interferents on the RTP signals of Mn-ZnS QDs. Some relevant anion ions (including NO_2^-, NO_3^-, SO_3^{2-}, SO_4^{2-}, CO_3^{2-}, I^-, Br^-, and SeO_3^{2-}) were detected (Fig. 5). The results showed that only selenite had a significant phosphorescence quenching effect on the Mn-ZnS QDs, indicating the high selectivity of the Mn-ZnS QDs for the detection and specific recognition of selenite in an aqueous solution.

Insert Fig. 5 here

3.5. Application in the detection of selenite in sodium selenite tablets

To illustrate the practical application of the RTP probe, recovery experiments were performed using the standard addition method in triplicate. The recovery of the spiked selenite was 94.7%-105.5%. All of the results are shown in Table 2. The probe was also applied to determine selenite in sodium selenite tablet and sodium selenite and vitamin E injection. As shown in Table 3, the analytical results for selenite are in good agreement with the labeled values. It can be concluded that the RTP probe is useful for the determination of selenite in real samples.

Insert Table 2 here

Insert Table 3 here

3.6. Quenching mechanism of Mn-ZnS QDs by selenite in the present of GSH

Selenite is commonly used as an inorganic dietary Se supplement. The reaction of selenite with GSH in organisms is of extreme importance, and has been studied extensively in detail [3, 5]. At ratios of 4:1 (GSH:selenite) or less, selenite is readily reduced by GSH to GSSeSG. When the GSH:selenite ratio exceeds 4:1, the GSSeSG is relatively unstable, and can be reduced to GSSeH and HSe^- [9, 52]. In this experiment, the optimal concentration of GSH exceeded 0.25 $mmol \cdot L^{-1}$ GSH, which was much larger than the concentration of selenite.

Some studies have shown that the luminescence of QDs can be altered by anions owing to the removal of the anion vacancies at the QDs surface [53, 54]. Wu et al. also showed that HSe^- ions are analogous in property and structure to S^{2-} ions, and are even more reactive toward Cd^{2+} than S^{2-} ions. They can also effectively interact with CdS QDs, and remove the S^{2-} vacancies on the particle surface [45]. As in our experiment, the HSe^- have the same effect on the Mn-ZnS QDs. And it might effectively quench the phosphorescence of the Mn-ZnS QDs.

To further understand the quenching mechanism in this experiment, the decay curves of the RTP emission of the Mn-ZnS QDs with and without selenite in the presence of GSH were investigated. As shown in Fig. 6, the RTP lifetime of Mn-ZnS QDs with selenite (0.702 ms) was shorter than the RTP lifetime of Mn-ZnS QDs (0.864 ms). This indicated that the addition of HSe^- resulted in an increased nonradiative decay of Mn-ZnS QDs [34, 53].

Insert Fig. 6 here

4. Conclusions

In summary, a new RTP probe was fabricated for the highly selective detection of selenite based on the RTP quenching effect by HSe^-, which were produced by the reaction of selenite and GSH. The RTP quenching of the Mn-ZnS QDs exhibited sensitive and selective responses to selenite. The proposed method was successfully applied for the determination of selenite in sodium selenite tablets and sodium selenite and vitamin E injection. We are able to determine the concentration of selenide in the range from micromolar to sub-micromolar levels, which is close to the optimal concentration of selenide needed for the growth of various bacterial species and cultures of mammalian cells. Moreover, the Mn-ZnS QDs presented a simple and feasible strategy to detect anion.

Acknowledgements

The authors are grateful for the financial support from the Natural Science Foundation of China (Nos. 21177102, 21577110).

References

[1] G.V. Kryukov, S. Castellano, S.V. Novoselov, A.V. Lobanov, O. Zehtab, R. Guigo, V.N. Gladyshev, Characterization of mammalian selenoproteomes, Science, 300 (2003) 1439-1443.

[2] L.V. Papp, J. Lu, A. Holmgren, K.K. Khanna, From selenium to selenoproteins: Synthesis, identity, and their role in human health, Antioxid Redox Sign, 9 (2007) 775-806.

[3] M. Roman, P. Jitaru, C. Barbante, Selenium biochemistry and its role for human health, Metallomics, 6 (2014) 25-54.

[4] M.P. Rayman, Selenium and human health, Lancet, 379 (2012) 1256-1268.

[5] Navarro-Alarcon, M., C. Cabrera-Vique, Selenium in food and the human body: A review, Sci Total Environ, 400 (2008) 115-141.

[6] E. Dumont, F. Vanhaecke, R. Cornelis, Selenium speciation from food source to metabolites: a critical review, Anal Bioanal Chem, 385 (2006) 1304-1323.

[7] M. Vinceti, S. Stranges, S. Sieri, S. Grioni, C. Malagoli, P. Muti, F. Berrino, V. Krogh, Association Between High Selenium Intake and Subsequent Increased Risk of Type 2 Diabetes in an Italian Population, Epidemiology, 20 (2009) S47-S47.

[8] H. Steinbrenner, B. Speckmann, A. Pinto, H. Sies, High selenium intake and increased diabetes risk: experimental evidence for interplay between selenium and carbohydrate metabolism, J Clin Biochem Nutr, 48 (2011) 40-45.

[9] R.J. Turner, J.H. Weiner, D.E. Taylor, Selenium metabolism in Escherichia coli, Biometals, 11 (1998) 223-227.

[10] C.M. Weekley, J.B. Aitken, S. Vogt, L.A. Finney, D.J. Paterson, M.D. de Jonge, D.L. Howard, P.K. Witting, I.F. Musgrave, H.H. Harris, Metabolism of Selenite in Human Lung Cancer Cells: X-Ray Absorption and Fluorescence Studies, J Am Chem Soc, 133 (2011) 18272-18279.

[11] T. Ishrat, K. Parveen, M.M. Khan, G. Khuwaja, M.B. Khan, S. Yousuf, A. Ahmad, P. Shrivastau, F. Islam, Selenium prevents cognitive decline and oxidative damage in rat model of streptozotocin-induced experimental dementia of Alzheimer's type, Brain Res, 1281 (2009) 117-127.

[12] M.A. Bryszewska, A. Mage, Determination of selenium and its compounds in marine organisms, J Trace Elem Med Bio, 29 (2015) 91-98.

[13] M. Deaker, W. Maher, Low volume microwave digestion for the determination of selenium in marine biological tissues by graphite furnace atomic absorption spectroscopy, Anal Chim Acta, 350 (1997) 287-294.

[14] J.F. Tyson, C.D. Palmer, Simultaneous detection of selenium by atomic fluorescence and sulfur by molecular emission by flow-injection hydride generation with on-line reduction for the determination of selenate, sulfate and sulfite, Anal Chim Acta, 652 (2009) 251-258.

[15] Z.F. Zhang, Y.M. Miao, Q.D. Zhang, G.Q. Yan, Facile and sensitive detection of protamine by enhanced room-temperature phosphorescence of Mn-doped ZnS quantum dots, Anal Biochem, 478 (2015) 90-95.

[16] Q. Jin, Y.L. Hu, Y.X. Sun, Y. Li, J.Z. Huo, X.J. Zhao, Room-temperature phosphorescence by Mn-doped ZnS quantum dots hybrid with Fenton system for the selective detection of Fe^{2+}, Rsc Adv, 5 (2015) 41555-41562.

[17] P. Wu, L.N. Miao, H.F. Wang, X.G. Shao, X.P. Yan, A Multidimensional Sensing Device for the Discrimination of Proteins Based on Manganese-Doped ZnS Quantum Dots, Angew Chem Int Edit, 50 (2011) 8118-8121.

[18] W.Y. Xie, W.T. Huang, H.Q. Luo, N.B. Li, CTAB-capped Mn-doped ZnS quantum dots and label-free aptamer for room-temperature phosphorescence detection of mercury ions, Analyst, 137 (2012) 4651-4653.
[19] C.H. Li, P. Wu, X.D. Hou, Plasma-assisted quadruple-channel optosensing of proteins and cells with Mn-doped ZnS quantum dots, Nanoscale, 8 (2016) 4291-4298.
[20] L.J. Sang, H.F. Wang, Aminophenylboronic-Acid-Conjugated Polyacrylic Acid-Mn-Doped ZnS Quantum Dot for Highly Sensitive Discrimination of Glycoproteins, Anal Chem, 86 (2014) 5706-5712.
[21] Y. Gong, Z.F. Fan, Room-Temperature Phosphorescence Turn-on Detection of DNA Based on Riboflavin-Modulated Manganese Doped Zinc Sulfide Quantum Dots, J Fluoresc, 26 (2016) 385-393.
[22] L. Dan, H.F. Wang, Mn-Doped ZnS Quantum Dot Imbedded Two-Fragment Imprinting Silica for Enhanced Room Temperature Phosphorescence Probing of Domoic Acid, Anal Chem, 85 (2013) 4844-4848.
[23] Q. Jin, Y. Li, J.Z. Huo, X.J. Zhao, The "off-on" phosphorescent switch of Mn-doped ZnS quantum dots for detection of glutathione in food, wine, and biological samples, Sensor Actuat B-Chem, 227 (2016) 108-116.
[24] X. Zhang, S. Yang, W.T. Zhao, L.Q. Sun, A.Q. Luo, Mn-doped ZnS QDs entrapped in molecularly imprinted membranes for detection of trace bisphenol A, Anal Methods-Uk, 7 (2015) 8212-8219.
[25] C.Y. Xu, R.H. Zhou, W.W. He, L. Wu, P. Wu, X.D. Hou, Fast Imaging of Eccrine Latent Fingerprints with Nontoxic Mn-Doped ZnS QDS, Anal Chem, 86 (2014) 3279-3283.
[26] P. Wu, X.P. Yan, Doped quantum dots for chemo/biosensing and bioimaging, Chem Soc Rev, 42 (2013) 5489-5521.
[27] W. Bian, J. Ma, W.R. Guo, D.T. Lu, M. Fan, Y.L. Wei, Y.F. Li, S.M. Shuang, M.M.F. Choi, Phosphorescence detection of L-ascorbic acid with surface-attached N-acetyl-L-cysteine and L-cysteine Mn doped ZnS quantum dots, Talanta, 116 (2013) 794-800.
[28] Z.F. Zhang, Y.M. Miao, Q.D. Zhang, L.W. Lian, G.Q. Yan, Selective room temperature phosphorescence detection of heparin based on manganese-doped zinc sulfide quantum dots/polybrene self-assembled nanosensor, Biosens Bioelectron, 68 (2015) 556-562.
[29] P. Wu, Y. He, H.F. Wang, X.P. Yan, Conjugation of Glucose Oxidase onto Mn-Doped ZnS Quantum Dots for Phosphorescent Sensing of Glucose in Biological Fluids, Anal Chem, 82 (2010) 1427-1433.
[30] H.F. Wang, Y. Li, Y.Y. Wu, Y. He, X.P. Yan, Ascorbic Acid Induced Enhancement of Room Temperature Phosphorescence of Sodium Tripolyphosphate-Capped Mn-Doped ZnS Quantum Dots: Mechanism and Bioprobe Applications, Chem-Eur J, 16 (2010) 12988-12994.
[31] H.F. Wang, Y.Y. Wu, X.P. Yan, Room-Temperature Phosphorescent Discrimination of Catechol from Resorcinol and Hydroquinone Based on Sodium Tripolyphosphate Capped Mn-Doped ZnS Quantum Dots, Anal Chem, 85 (2013) 1920-1925.
[32] H.B. Ren, X.P. Yan, Ultrasonic assisted synthesis of adenosine triphosphate capped manganese-doped ZnS quantum dots for selective room temperature phosphorescence detection of arginine and methylated arginine in urine based on supramolecular Mg^{2+}-adenosine triphosphate-arginine ternary system, Talanta, 97 (2012) 16-22.
[33] Y. He, H.F. Wang, X.P. Yan, Exploring Mn-doped ZnS quantum dots for the room-temperature phosphorescence detection of enoxacin in biological fluids, Anal Chem, 80 (2008) 3832-3837.
[34] H.B. Ren, B.Y. Wu, J.T. Chen, X.P. Yan, Silica-Coated S^{2-}-Enriched Manganese-Doped ZnS Quantum Dots as a Photoluminescence Probe for Imaging Intracellular Zn^{2+} Ions, Anal Chem, 83 (2011)

8239-8244.
[35] H.F. Wang, Y. He, T.R. Ji, X.P. Yan, Surface Molecular Imprinting on Mn-Doped ZnS Quantum Dots for Room-Temperature Phosphorescence Optosensing of Pentachlorophenol in Water, Anal Chem, 81 (2009) 1615-1621.
[36] X. Wei, Z.P. Zhou, T.F. Hao, H.J. Li, Y.Q. Xu, K. Lu, Y.L. Wu, J.D. Dai, J.M. Pan, Y.S. Yan, Highly-controllable imprinted polymer nanoshell at the surface of silica nanoparticles based room-temperature phosphorescence probe for detection of 2,4-dichlorophenol, Anal Chim Acta, 870 (2015) 83-91.
[37] H. Wu, Z.F. Fan, Mn-doped ZnS quantum dots for the room-temperature phosphorescence detection of raceanisodamine hydrochloride and atropine sulfate in biological fluids, Spectrochim Acta A, 90 (2012) 131-134.
[38] Y.M. Miao, M.Q. Yang, G.Q. Yan, Self-assembly of phosphorescent quantum dots/boronic-acid-substituted viologen nanohybrids based on photoinduced electron transfer for glucose detection in aqueous solution, Rsc Adv, 6 (2016) 8588-8593.
[39] Z.F. Zhang, Y.M. Miao, L.W. Lian, G.Q. Yan, Detection of quercetin based on Al^{3+}-amplified phosphorescence signals of manganese-doped ZnS quantum dots, Anal Biochem, 489 (2015) 17-24.
[40] X. Wei, Z.P. Zhou, T.F. Hao, H.J. Li, Y.S. Yan, Molecularly imprinted polymer nanospheres based on Mn-doped ZnS QDs via precipitation polymerization for room-temperature phosphorescence probing of 2,6-dichlorophenol, Rsc Adv, 5 (2015) 19799-19806.
[41] P. Wu, T. Zhao, Y.F. Tian, L. Wu, X.D. Hou, Protein-Directed Synthesis of Mn-Doped ZnS Quantum Dots: A Dual-Channel Biosensor for Two Proteins, Chem-Eur J, 19 (2013) 7473-7479.
[42] Y.M. Miao, Y.T. Li, Z.F. Zhang, G.Q. Yan, Y. Bi, "Turn off-on" phosphorescent biosensors for detection of DNA based on quantum dots/acridine orange, Anal Biochem, 475 (2015) 32-39.
[43] L. Tan, C.C. Rang, S.Y. Xu, Y.W. Tang, Selective room temperature phosphorescence sensing of target protein using Mn-doped ZnS QDs-embedded molecularly imprinted polymer, Biosens Bioelectron, 48 (2013) 216-223.
[44] Y.M. Miao, Application of BSA-bioconjugated phosphorescence nanohybrids in protein detection in biofluids, Rsc Adv, 5 (2015) 76804-76812.
[45] C.L. Wu, Y.B. Zhao, CdS quantum dots as fluorescence probes for the sensitive and selective detection of highly reactive HSe^- ions in aqueous solution, Anal Bioanal Chem, 388 (2007) 717-722.
[46] J.Q. Zhuang, X.D. Zhang, G. Wang, D.M. Li, W.S. Yang, T.J. Li, Synthesis of water-soluble ZnS : Mn^{2+} nanocrystals by using mercaptopropionic acid as stabilizer, J Mater Chem, 13 (2003) 1853-1857.
[47] J.H. Chung, C.S. Ah, D.J. Jang, Formation and distinctive decay times of surface- and lattice-bound Mn^{2+} impurity luminescence in ZnS nanoparticles, J Phys Chem B, 105 (2001) 4128-4132.
[48] S.Y. Cui, H. Jin, S.J. Kim, A.P. Kumar, Y.I. Lee, Interaction of glutathione and sodium selenite in vitro investigated by Electrospray ionization tandem mass spectrometry, J Biochem, 143 (2008) 685-693.
[49] H. Ibrahim, Y.M. Issa, O.R. Shehab, New selenite ion-selective electrodes based on 5,10,15,20-tetrakis-(4-methoxyphenyl)-21H,23H-porphyrin-Co(II), J Hazard Mater, 181 (2010) 857-867.
[50] S.D. Noblitt, L.C. Staicu, C.J. Ackerson, C.S. Henry, Sensitive, Selective Analysis of Selenium Oxoanions Using Microchip Electrophoresis with Contact Conductivity Detection, Anal Chem, 86 (2014) 8425-8432.

[51] I. Ipolyi, Z. Stefanka, P. Fodor, Speciation of Se(IV) and the selenoamino acids by high-performance liquid chromatography-direct hydride generation-atomic fluorescence spectrometry, Anal Chim Acta, 435 (2001) 367-375.
[52] C.B. Huang, C.L. Wu, J.P. Lai, S.Y. Li, J.S. Zhen, Y.B. Zhao, CdS quantum dots as fluorescence probes for the detection of selenite, Anal Lett, 41 (2008) 2117-2132.
[53] X.C. Wu, A.M. Bittner, K. Kern, Synthesis, photoluminescence, and adsorption of CdS/dendrimer nanocomposites, J Phys Chem B, 109 (2005) 230-239.
[54] P.V. Kamat, B. Patrick, Photophysics And Photochemistry Of Quantized Zno Colloids, J Phys Chem-Us, 96 (1992) 6829-6834.

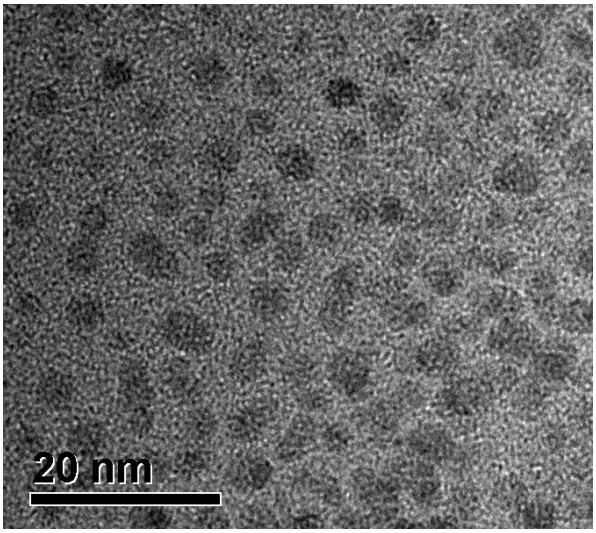

Fig. 1 HRTEM image of Mn-ZnS QDs.

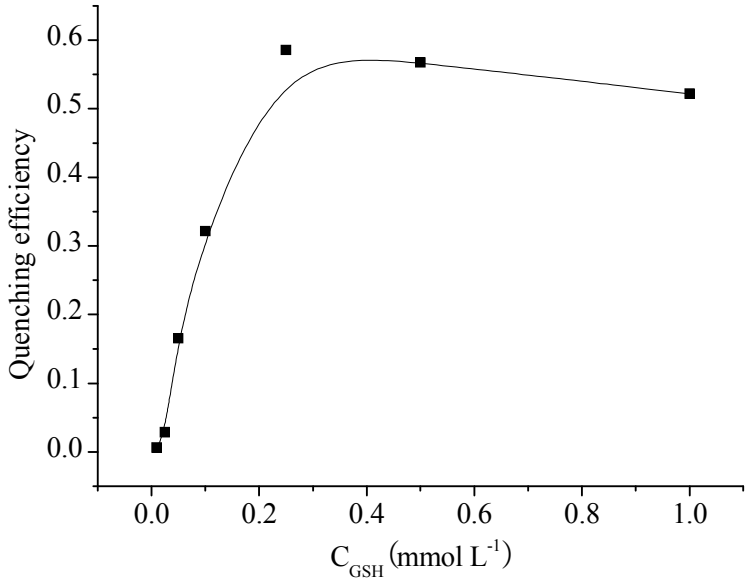

Fig. 2 Quenching efficiency of Mn-ZnS QDs in the presence of selenite with various concentrations of GSH.

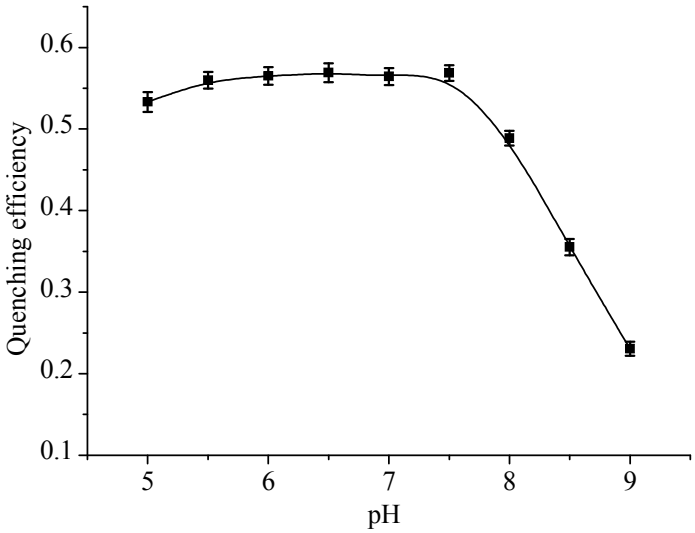

Fig. 3 Effect of the pH on the quenching efficiency of the Mn-ZnS QDs in the presence of 0.25 mmol·L^{-1} GSH and 5 μmol·L^{-1} selenite

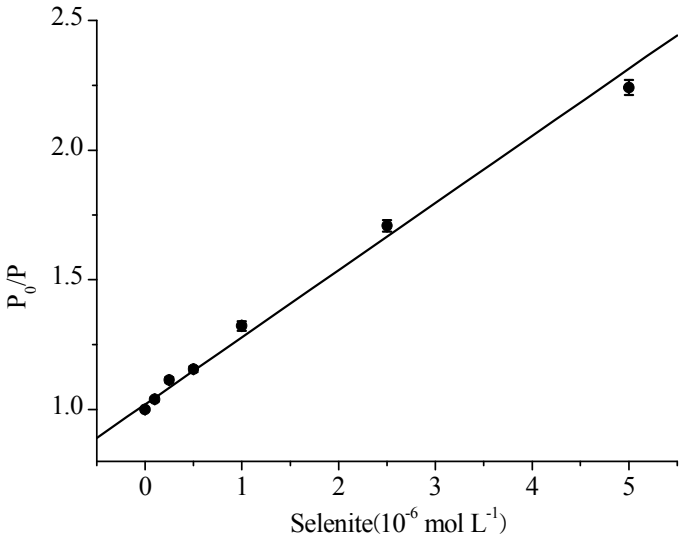

Fig. 4 Linear plots of P_0/P against different selenite concentrations (where P_0 and P were the RTP intensity of the Mn-ZnS QDs with GSH in the absence and presence of selenite).

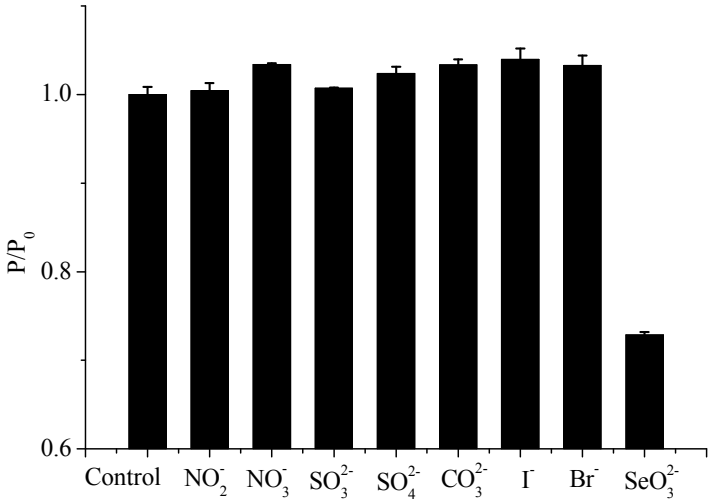

Fig. 5 Selectivity of Mn-ZnS toward selenite (performed in 10 mmol·L^{-1} Tris-HCl buffer at a pH of 7.4; the concentrations of selenite was 1.0 μmol·L^{-1}; the concentrations of all of the other anion ions were 100 μmol·L^{-1}; the P_0 and P were the RTP intensity of the Mn-ZnS QDs with GSH in the absence and presence of anion ions.)

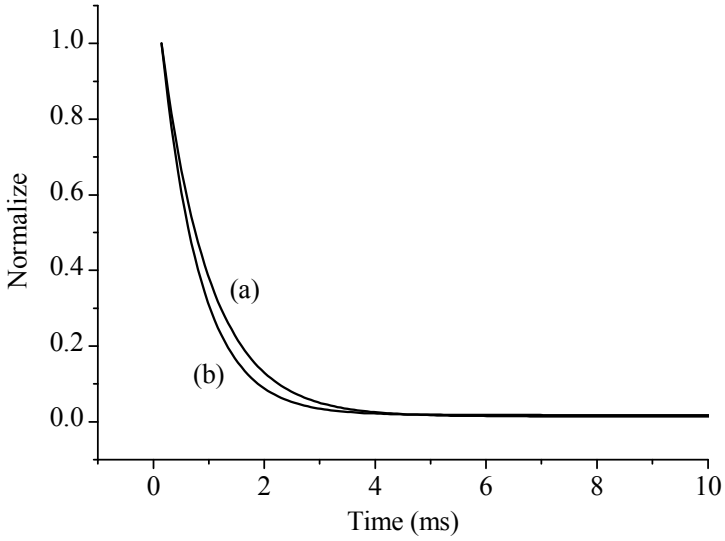

Fig. 6 Decay curves of the RTP emission of Mn-ZnS QDs before (a) and after addition of 5 μmol·L^{-1} selenite (b) in 10 mmol·L^{-1} Tris-HCl buffer at a pH of 7.4.

Table 1 Comparison of the proposed method with different analytical techniques reported for detection of selenite

Sensing system	Linear range ($mol \cdot L^{-1}$)	Detection limit ($mol \cdot L^{-1}$)	Ref.
PVC membrane electrode	5.5×10^{-5}- 1.0×10^{-2}	3.4×10^{-5}	[49]
Microchip capillary electrophoresis	1.0×10^{-6}- 5.0×10^{-4}	3.8×10^{-7}	[50]
Atomic fluorescence spectrometry	2.0×10^{-7}- 1.3×10^{-3}	2.0×10^{-7}	[51]
Mn-ZnS QDs	1.0×10^{-7}- 5.0×10^{-6}	8.5×10^{-8}	This work

Table 2 Recovery for the determination of selenite

Spiked selenite ($\mu mol \cdot L^{-1}$)	Detection value ($\mu mol \cdot L^{-1}$)			Recovery
0.50	0.47	0.46	0.49	94.7%±2.5%
1.00	1.02	1.05	1.03	103.3%±1.2%
2.50	2.62	2.71	2.58	105.5%±2.2%

Table 3 Determination of selenite in real samples

Sample type	Labeled ($mg \cdot tablet^{-1}$, $mg \cdot mL^{-1}$)	Found ($mg \cdot tablet^{-1}$, $mg \cdot mL^{-1}$)
Sodium selenite tablets 1	0.2	0.195±0.008
Sodium selenite tablets 2	1.0	1.037±0.032
Sodium selenite and vitamin E injection	1.0	0.968±0.028

Table of contents

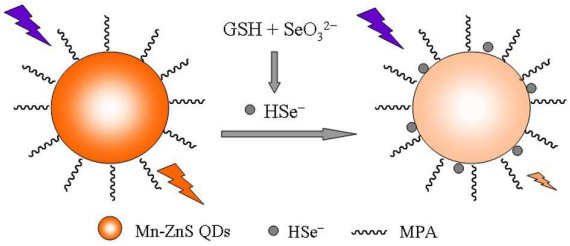

Selenite was selectively and sensitively detected based on the room-temperature phosphorescence quenching of Mn-ZnS QDs caused by HSe^- from the reaction of selenite and glutathione.